

# VALIDATED EQUIVALENT SOURCE MODEL FOR AN UNDER-EXPANDED HYDROGEN JET

Hecht, E.S.<sup>1</sup>, Li, X.<sup>2</sup>, and Ekoto, I.W.<sup>1</sup>

<sup>1</sup>Combustion Research Facility, Sandia National Laboratories, Livermore, CA, USA, ehecht@sandia.gov, iekoto@sandia.gov

<sup>2</sup>Department of Thermal Engineering, Tsinghua University, Beijing, China, lixfthu@163.com

## ABSTRACT

As hydrogen fuel cell vehicles become more widely adopted by consumers, the demand for refueling stations increases. Most vehicles require high-pressure (either 350 or 700 bar) hydrogen, and therefore the refueling infrastructure must support these pressures. Fast running, reduced order physical models of releases from high-pressure sources are needed so that quantitative risk assessment can guide the safety certification of these stations. A release from a high pressure source is choked at the release point, forming the complex shock structures of an under-expanded jet before achieving a characteristic Gaussian profile for velocity, density, mass fraction, etc. downstream. Rather than using significant computational resources to resolve the shock structure, an equivalent source model can be used to quickly and accurately describe the flow in terms of velocity, diameter, and thermodynamic state after the shock structure. In this work, we present correlations for the equivalent boundary conditions of a subsonic jet as a high-pressure jet, downstream of the shock structure. Schlieren images of under-expanded jets are used to show that the geometrical structure of under-expanded jets scale with the square root of the static to ambient pressure ratio. Correlations for an equivalent source model are given, and these parameters are also found to scale with square root of the pressure ratio. We present our model as well as planar laser Rayleigh scattering validation data for static pressures up to 60 bar.

## 1 INTRODUCTION

There are already several hundred hydrogen fuel cell vehicles on the road in California, with more automakers offering vehicles for public lease and sale in 2015 [1]. However, there are currently only 8 public fueling stations open in California, and this is more than any other region in the world [1]. There is an obvious need for fueling station infrastructure to expand to make this technology viable, but the codes and standards that govern the permitting of this infrastructure often make it challenging to place the necessary equipment in densely populated areas and/or alongside gasoline dispensing equipment [2].

Quantitative risk assessment (QRA) is an effective way to inform the fire codes and give authorities confidence in approving a given design [3]. Effective QRA requires involves the modeling of many failures (i.e. leaks), as well as the hazards and harm. The large number of scenarios that must be modeled for QRA requires fast-running, reduced-order models, rather than computationally

expensive simulations, such as computational fluid dynamics (CFD) with a fine mesh. This work focuses on one portion of a hydrogen leak scenario that is critical to modeling the entire scenario: the physics of the initial expansion of a hydrogen leak, with targeted experiments to develop a reduced-order model for this region of a hydrogen leak. The model for this expansion region can provide boundary conditions to CFD simulations or an integral model that is one-dimensional along the streamline, but can still account for the trajectory curvature due to buoyancy or wind (which is a more feasible simulation for QRA).

When the pressure ratio across an orifice is above the critical ratio ( $\approx 1.9$  for hydrogen), the flow chokes, meaning that it is sonic through the throat, but remains at a higher pressure than the outlet pressure. As the flow expands downstream of the throat and the pressure drops to the outlet pressure, shock structures form in the flow. For circular jets, a barrel shock typically extends from the orifice edges up to the normal, Mach disk shock. This barrel shock is surrounded by a supersonic slip region, and downstream of the Mach disk, reflected shocks can often be observed. These shock structures have been well studied in the literature, for gases including air, nitrogen, argon, helium, CO<sub>2</sub>, and natural gas [4–9]. Studies using hydrogen are less common, although the same barrel shock, Mach disk, and diamond reflection structures are observed, even for non-circular orifices [10, 11]. While it is possible to model the compressible flow structures of an under-expanded jet, it is generally computationally intensive, due to the fine computational mesh required to achieve grid independence [12]. Even for CFD simulations, this computational expense can be too great, and it is more effective to use a notional nozzle, or equivalent source model for the release.

Downstream of the shock structure of super-critical flows, canonical hyperbolic centerline decay rates of the velocity, concentration, etc., for sub-critical flows are observed for under-expanded jets. The cross-sectional profiles of these fields (normal to the flow direction) are also observed to be Gaussian, and collapse onto a single curve when normalized properly. This has led a number of authors to derive notional nozzle models that relate the actual source to an equivalent sub-critical source. However, these notional nozzle models are typically only used to scale the centerline concentration or velocity decay rate, rather than to generate boundary conditions to a CFD or reduced-order model. This work presents correlations to produce boundary conditions for an equivalent sub-sonic source as a high-pressure source that would generate the observed downstream conditions.

Birch et al. [6] were one of the first to develop a model for the high-pressure expansion region, which conserved mass between the source and pseudo-source, with an assumption that the pseudo-source was at the storage temperature and sonic velocity. This work was slightly modified by Ewan and Moodie [7], who assumed that the temperature of the pseudo-source was the throat temperature. Birch et al. [13] followed up their previous work by conserving mass and momentum between the source and pseudo-source for a better prediction of the velocity after the shock. Yüceil and Ötügen [9] conserved mass, momentum, and energy, removing the assumptions on the pseudo-source temperature. Harstad and Bellan [14] derived a model that assumes that all of the flow is through the Mach disk and considers the entropy that is generated across this normal shock, as the supersonic flow becomes subsonic. Molkov [15] derived a model that conserved mass and energy between the source and pseudo-source, using the Abel-Nobel equation of state. Many of these models were updated to use the more relevant Abel-Nobel equation of state, and the range of pseudo-sources predicted for a given flow condition are shown by Ruggles and Ekoto [10]. The effect of the notional nozzle model on the predictions of a flame length and trajectory can also be seen in [16]. With the large variation in predictions of these models, there is a critical need to eliminate ambiguity and validate the use of a single model to describe hydrogen expansion, especially if these models are to be used for QRA.

Table 1: Experimental conditions.

Stagnation pressure (bar)	Nozzle exit density (kg/m <sup>3</sup> )
10	0.564
30	1.589
50	2.614
60	3.126

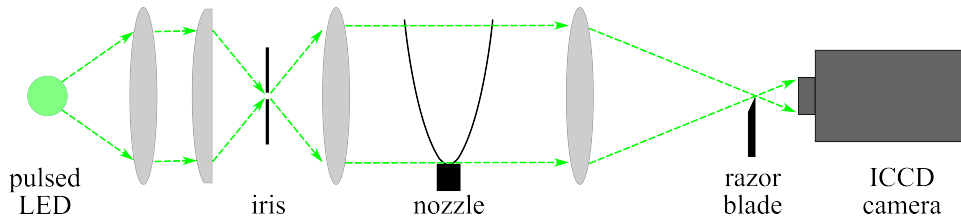


Figure 1: Schematic of inline schlieren imaging setup.

## 2 EXPERIMENTAL SETUP

A custom designed high-pressure stagnation chamber with an internal volume of 1.24 L was used to create the under-expanded hydrogen jets with static pressures up to 60 bar. To obtain data of different flow scales, a set of interchangeable nozzles with diameters range from 0.5 mm to 1.5 mm were attached to the stagnation chamber. Long radius nozzle profiles from ASME MFC-3M-2004 were selected to produce uniform exit velocity profiles. The gas temperature was monitored using a type K thermal couple, while the chamber pressure was measured with a TESCO series 100 pressure transducer. To maintain a steady stagnation pressure inside the chamber, dynamic feedback was employed. Further details of the stagnation chamber and the nozzle profile can be found in [10].

In this work, under-expanded hydrogen jets with a series of pressure ratios using different nozzles were studied. The experimental conditions are shown in Table 1. All the pressure ratios in this study resulted in a choked flow at the nozzle exit. The nozzle exit density at a given pressure ratio was calculated using an isentropic flow relationship, assuming the gas would flow at the sonic velocity. During the experiments, the room temperature and pressure were 1 bar and 294 K.

To study the expansion region of these under-expanded hydrogen jets, two diagnostics were employed on the high-pressure releases of hydrogen. First, schlieren imaging was used to spatially quantify the shock structures and qualitatively understand the flows in the region near the orifice. A sketch of the in-line lens based schlieren imaging system is shown in Fig. 1. A custom built light-emitting diode (LED) light source with a fixed 520 nm wavelength, with a pulse duration of 5  $\mu$ s was used for illumination. The short pulse duration allows for the resolution of turbulent flow structures in the schlieren images. A Princeton Instruments PI-MAX intensified camera was used to record the shock structures. Before turning on the LED light, 50 background images,  $Bg(x, y)$ , were taken. Then, for each nozzle and pressure combination, 80 images were recorded with the LED light on but no nozzle flow (pure air images) to determine the optical response,  $Or(x, y)$ , which was the difference between the air images and the mean background response. Finally, 200 instantaneous images,  $R(x, y)$  were recorded. The data reduction algorithm is expressed mathematically

in the following equation:

$$i(x, y) = \frac{R(x, y) - \overline{Bg}(x, y)}{\overline{Or}(x, y)}, \quad (1)$$

where  $i(x, y)$  is the final schlieren image, and the vinculum denotes the time averaged image.

The second diagnostic employed on these under-expanded hydrogen jets was Planar Laser Rayleigh Scattering (PLRS), which was used to quantify the concentration of hydrogen downstream of the shock structure. The PLRS setup is the similar to that described by Ruggles and Ekoto [10]. Briefly, a Nd:YAG laser (frequency doubled to 532 nm, with  $\approx 9$ ns pulse duration,  $\approx 1$ J/pulse) was formed into a sheet approximately 40 mm high. During these experiments, due to the large spreading area of the hydrogen, two cameras were placed perpendicular to the laser sheet, and the timing was synchronized. A Princeton Instruments PIXIS 400B camera with an  $f1.2$  Nikon 50 mm lens and a Nikon 3T close up lens were used to image the region with hydrogen. A Princeton Instruments PI-MAX intensified camera with a  $f1.4$  Nikon 50 mm lens mounted on 12mm extension ring was used to image a region with pure air, adjacent to the hydrogen jet. The jet was traversed vertically in 30 mm increments, and between 3-5 regions were imaged for each condition tested to give an overall field of view of 100-160 mm.

Before the under-expanded jet experiments, a correction for the non-linear gain and flat-field response of the PI-MAX camera was generated using the method described by Williams and Shaddix [17]. Each of the images taken by the PI-MAX camera were corrected for these effects. Experimental calibration involved capturing 800 images of pure air, and 800 images of pure helium using the PIXIS 400B camera, while capturing the same number of images, always of pure air, with the PI-MAX ICCD camera. The images taken by the PI-MAX camera were corrected and then integrated in the horizontal ( $x$ ) direction to determine the proportionality constant of the laser power at a given  $y$  position for an image set,  $St_i(y)$ , where the subscript  $i$  denotes a single image. These corrected images were also integrated in both spatial directions to determine an overall laser shot power,  $p_i$ . The optical response of the system was calculated through the relationship:

$$Or(x, y) = \frac{\sum p_{i, \text{He}} (\sum (R_{i, \text{air}}(x, y) - \overline{Bg}(x, y))) - (\sum (R_{i, \text{He}}(x, y) - \overline{Bg}(x, y)))}{\sum p_{i, \text{air}} \sum St_{i, \text{air}}(y) - \frac{\sigma_{\text{He}}}{\sigma_{\text{air}}} \sum St_{i, \text{He}}(y)}, \quad (2)$$

where the scattering cross-section of air relative to helium,  $\sigma_{\text{He}}/\sigma_{\text{air}}$  is 1/71.648. Imaging experiments required the capture of 800 images of pure air (along with 50 images without the laser firing to measure the background,  $Bg$ , signal) to calculate the back-scatter of laser light:

$$s_b(x, y) = \frac{1}{\sum p_i} \left( \frac{\sum (R_{i, \text{air}}(x, y) - \overline{Bg}(x, y))}{Or(x, y)} - \sum St_i(y) \right), \quad (3)$$

where the summations are over the 800 images (subscript  $i$ ). Finally, the intensity of Rayleigh scatter, proportional to the mole fraction of hydrogen was calculated for each image through the relationship:

$$I_i(x, y) = \frac{1}{St_i(y)} \left[ \frac{R_i(x, y) - \overline{Bg}(x, y)}{OR(x, y)} - s_b(x, y) \cdot p_i \right]. \quad (4)$$

Mole fractions were calculated from the calibrated helium and air data, and the known scattering cross-section differences for helium and hydrogen ( $\sigma_{\text{H}_2} = 15.96\sigma_{\text{He}}$ ) by using the helium data to predict a scattering intensity for hydrogen, and then finding the mole fraction:

$$\chi = \frac{I_{\text{air}}(x, y) - I(x, y)}{I_{\text{air}}(x, y) - I_{\text{H}_2}(x, y)}. \quad (5)$$

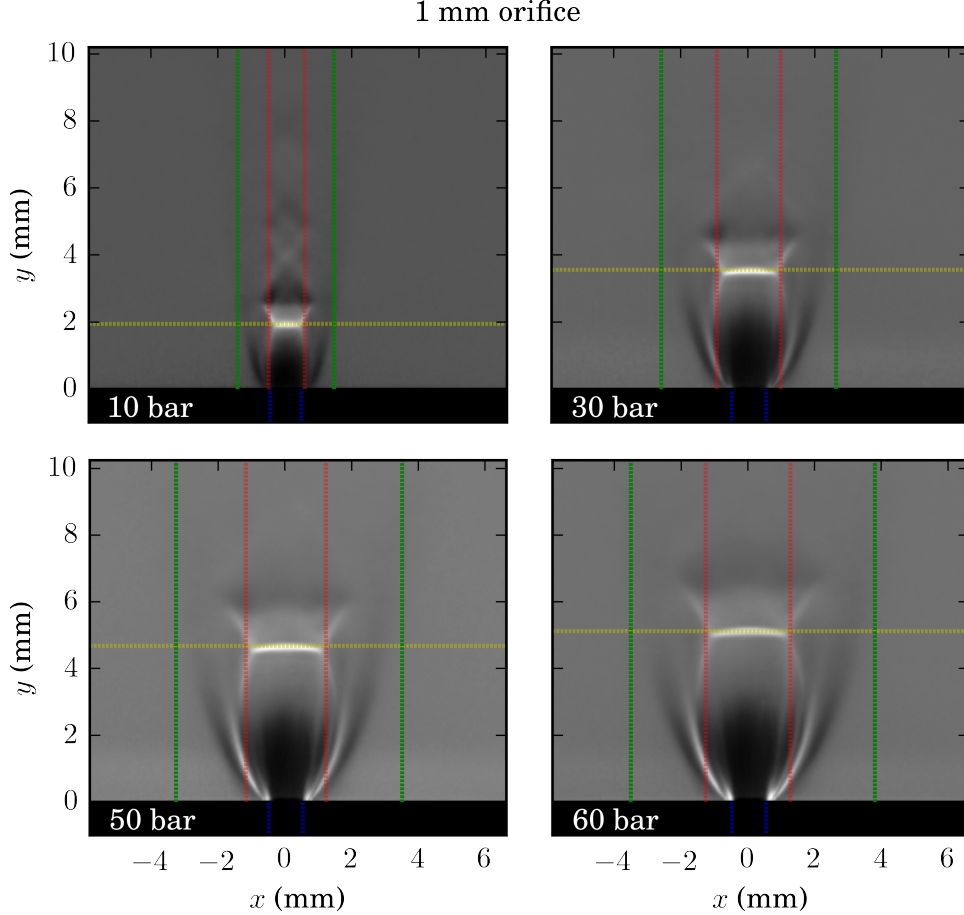


Figure 2: Schlieren images of hydrogen issuing through a 1 mm orifice at various storage pressures. The dashed yellow line shows the  $y$  location of the Mach disk, the red lines show the edges of the disk, and the green lines show the edges of the slip region at the Mach disk.

### 3 UNDER-EXPANDED JET SHOCK STRUCTURE

Schlieren images are formed due to refraction index changes in fluids. The refraction index of a fluid can change due to its composition, temperature, density or pressure. Schlieren imaging to quantify the density in the near-field of an under-expanded jet is challenging, since the temperature, pressure, and density are all varying spatially, and there is air entrainment near the edges, causing composition changes. Schlieren is also a line-of-site measurement, and gives only an integrated refraction index change across the flow field. In this work, we forewent the challenge of quantifying the composition and state of the jet shock structure, but did quantify the spatial locations of the jet features in the schlieren images.

Figure 2 is a typical series of mean schlieren images for hydrogen issuing through a 1 mm orifice. Traditional features of an under-expanded jet are clear in these images. The Mach disk is a bright white region in the images and diamond-shaped reflected shocks are observed downstream of the Mach disk. The barrel shock can be observed extending from the nozzle up to the Mach disk, and outer compression waves can be seen extending from the orifice outside the barrel shock. There is

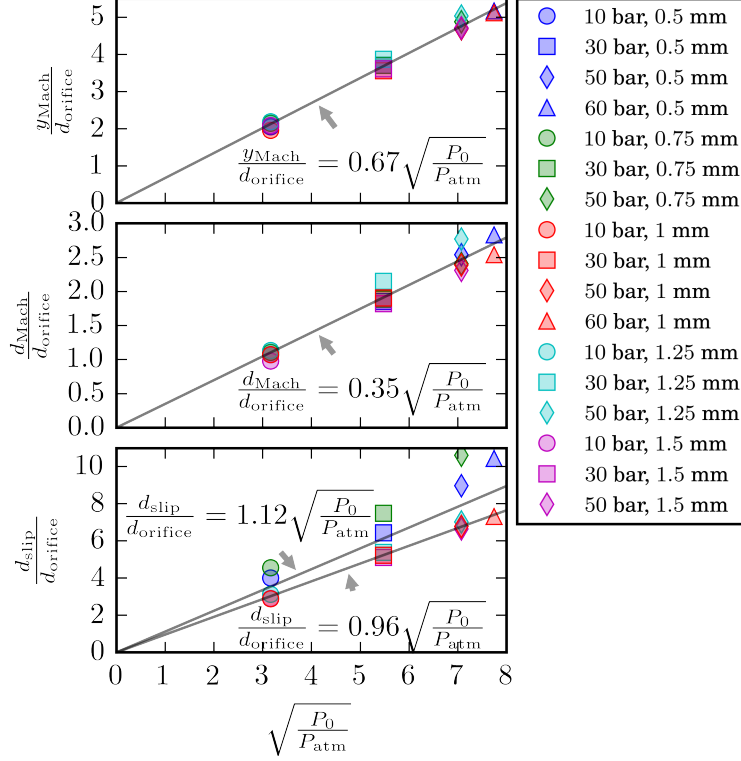


Figure 3: Geometry of an under-expanded hydrogen jet. Top frame shows the standoff distance of the Mach disk relative to the orifice diameter, middle frame shows the relative Mach disk diameter, and the bottom frame shows the relative diameter of the slip region (including the Mach disk). Linear fits to the square root of the pressure ratio are shown. In the bottom frame, the top fit is to all of the data, while the bottom fit is for the data only where the orifice diameter is  $\geq 1$  mm.

also evidence of the Mach disk moving further downstream and all of the features increasing in size as the stagnation pressure increases.

To quantify the downstream location of the Mach disk, and the size of the Mach disk and slip regions, a schlieren image processing routine was developed. The downstream location of the Mach disk was calculated as the maximum image intensity value along the  $x = 0$  axis. The edges of the Mach disk were found as the maximum gradient of the image intensity in the  $x$ -direction at the Mach disk  $y$ -location ( $\pm 5$  pixels). Finally, the edges of the slip region were defined as the location where the gradient of the image intensity or the gradient of the RMS image intensity in the  $x$ -direction at the Mach disk  $y$ -location first (coming from the edges) exceeded a threshold value. The automatically calculated Mach disk downstream location, edges, and edges of the slip region are shown for the 1 mm orifice in Fig. 2 as yellow, red, and green dashed lines, respectively.

The Mach disk location ( $y_{\text{Mach}}$ ), Mach disk diameter ( $d_{\text{Mach}}$ ), and diameter of the slip region ( $d_{\text{slip}}$ ) were calculated for each of the schlieren image series, and are shown in Fig. 3. The geometry of these under-expanded hydrogen jet features are normalized to the diameter of the orifice, and plotted as a function of the square root of the static to ambient pressure ratio. Many authors have shown that the Mach disk location scales as the square root of the pressure ratio [5, 18, 19], finding a scaling factor near 0.67. The linear fit to our data shown in Fig. 3 shows that this correlation holds true for under-expanded hydrogen jets. The Mach disk diameter and slip region

diameter also appear to scale linearly with respect to  $\sqrt{P_0/P_{\text{atm}}}$ . Two fits are shown in Fig. 3 for the diameter of the slip region. The upper correlation, with a scaling constant of 1.12 is a fit to all of the data, while the lower fit, with a scaling factor of 0.96 is a fit to the data only where the orifice diameter was  $\geq 1$  mm. The shock structures for releases from the 0.5 and 0.75 mm orifices were observed to be crooked, and errors in machining these small diameter orifices were suspected. While these machining errors appear not to have affected the Mach disk geometry significantly (the data points nearly all fall on the same line), we suspect that the crooked nozzles did significantly affect the slip region boundaries, and have more confidence in the lower correlation, where  $d_{\text{slip}}/d_{\text{orifice}} = 0.96\sqrt{P_0/P_{\text{atm}}}$ .

The original goal of this work was to use these geometrical correlations with the model proposed by Harstad and Bellan [14] to calculate the flow through the Mach disk, and the model proposed by Yüceil and Ötügen [9], updated to allow air entrainment to calculate the flow through the slip region as a two-zone notional nozzle model. This required an additional flow development region where the two annular plug-flows developed into a fully Gaussian subsonic jet profiles. Mass, momentum, and energy were conserved in each of the different regions, with an attempt to find empirical parameters for the length of the development region and the entrainment rate of air in the development region. However, we were unable to come up with any empirical parameters that gave reasonable predictions of the concentration fields measured during the Rayleigh experiments, and this approach was abandoned.

#### 4 EQUIVALENT SOURCE MODEL

The ultimate necessity of the equivalent source model is to provide boundary conditions to a model, whether that model be CFD (with the desire to decrease mesh resolution and computational requirements), or a reduced order model, as considered here. The equivalent source model herein was developed to provide boundary conditions to the first-order jet model described by Houf and Schefer [20]. Briefly, the jet velocity and density are assumed to have Gaussian profiles in the radial direction (normal to the jet centerline), as

$$u = u_{\text{cl}}(S) \exp \left[ - \left( \frac{r}{B} \right)^2 \right], \quad (6)$$

$$\rho = \rho_{\infty} - (\rho_{\infty} - \rho_{\text{cl}}(S)) \exp \left[ - \left( \frac{r}{\lambda B} \right)^2 \right]. \quad (7)$$

In these equations,  $u$  is the velocity,  $S$  is the streamline coordinate,  $r$  is the radial coordinate, the subscript cl denotes along the centerline ( $r = 0$ ), the subscript  $\infty$  denotes the atmospheric, far-field conditions,  $\rho$  is the density,  $B$  is a characteristic jet width and  $\lambda$  is the relative spreading ratio between the velocity and density fields, assumed to be 1.16 in this work. The hydrogen and air are assumed to behave as ideal gases at the same temperature, and the profile for the mass fraction of hydrogen ( $Y$ ) can be calculated as

$$\rho Y = \rho_{\text{cl}}(S) Y_{\text{cl}}(S) \exp \left[ - \left( \frac{r}{\lambda B} \right)^2 \right]. \quad (8)$$

With these assumed profiles, the differential conservation equations (along the streamline) for mass, momentum (including gravity), and species are written, with entrainment adding air to the mass of the jet. The entrainment is modeled with two contributions, one from momentum, which is a

function of the initial jet diameter, and the second from buoyancy, which is a function of the local Froude number. The boundary conditions needed for this model are the initial position ( $S_0$ ), density ( $\rho_{cl,0}$ ), velocity ( $u_{cl,0}$ ), mass fraction hydrogen ( $Y_{cl,0}$ ), and the initial characteristic jet width ( $B_0$ ). The effective diameter is also needed to calculate the momentum driven entrainment. Because the gases in the plume are assumed to behave as ideal gases at the same temperature and pressure, the density and mass fraction are related through the relationship

$$Y = \frac{M_{H_2}}{M_{air} - M_{H_2}} \left( \frac{\rho_\infty}{\rho} - 1 \right), \quad (9)$$

where  $M$  is the molecular weight.

By further assuming that the flow through the leak occurs at the sonic velocity, in a plug-flow manner, conservation equations for the hydrogen mass and momentum in the expansion region of the under-expanded jet are used to further reduce the number of fit parameters in this equivalent source model. At the leak, hydrogen is assumed to expand isentropically to the speed of sound. A non-ideal gas equation of state is used for this calculation, using the CoolProp Python library [21] to iteratively solve for the state at the throat. Once the state and speed of sound at the throat are known, the hydrogen mass flow and momentum balances between the throat and the start of the subsonic jet can be written as:

$$\frac{d_{throat}^2 \rho_{throat} u_{throat}}{4} = \rho_{cl,0} u_{cl,0} Y_{cl,0} B_0^2 \frac{\lambda^2}{\lambda^2 + 1} \quad (10)$$

$$\frac{d_{throat}^2 \rho_{throat} u_{throat}^2}{4} = u_{cl,0}^2 B_0^2 \frac{2\lambda^2 \rho_{cl,0} + \rho_\infty}{4\lambda^2 + 2}. \quad (11)$$

Solving these two equations for  $u_{cl,0}$ , and  $B_0$  as a function of  $\rho_{cl,0}$  leaves three unknowns to define the boundary conditions of the first-order jet model:  $\rho_{cl,0}$ ,  $S_0$ , and  $d_{eff}$ , where  $d_{eff}$  is the effective initial diameter used in the entrainment model.

As described in section 2, PLRS imaging was used to measure the mole fraction of under-expanded jets in the region downstream of the shock structure. These measurements showed the canonical hyperbolic centerline decay rates and collapsible Gaussian radial profiles for mole fraction that would be expected from a subsonic jet. The subsonic jet model was written in Python, and an error equation was cast, where the total error was calculated using the relationship:  $\epsilon = \sum_{x,y} (\chi_{measured}(x,y) - \chi_{calculated}(x,y))^2$ , with  $\chi$  as the mole fraction. Note that in the  $S$  and  $r$  coordinates from the jet model map directly to  $y$  and  $x$  for the vertical plumes studied. A differential evolution algorithm [22], followed by a basin hopping algorithm [23] were used to find the minimum error between the measured and calculated mole fraction fields as the three parameters ( $\rho_{cl,0}$ ,  $S_0$ , and  $d_{eff}$ ) were varied. The density,  $\rho_{cl,0}$ , was constrained to lie between the density of air and hydrogen, at room temperature and pressure. The starting position  $S_0$  (or  $y_{eff}$ ) and the effective diameter,  $d_{eff}$  were both constrained to lie between 0 and  $10\sqrt{P_0/P_\infty}$ . This constrained the starting position to be no more than 15 times the Mach disk downstream position, and the starting diameter to be no more than 30 times the Mach disk diameter. Two of the example measured and calculated best-fit mole fraction fields are shown in Fig. 4. As shown, the subsonic jet model predicts the mean mole fraction field reasonably well using the error-minimized boundary conditions.

The disagreement between the calculated and measured fields in Fig. 4 is due to several model parameters that have significant uncertainty [24]. The relative velocity to density spreading ratio,  $\lambda$  (assumed to be 1.16) can have a large influence on the width of the Gaussian profiles. Without

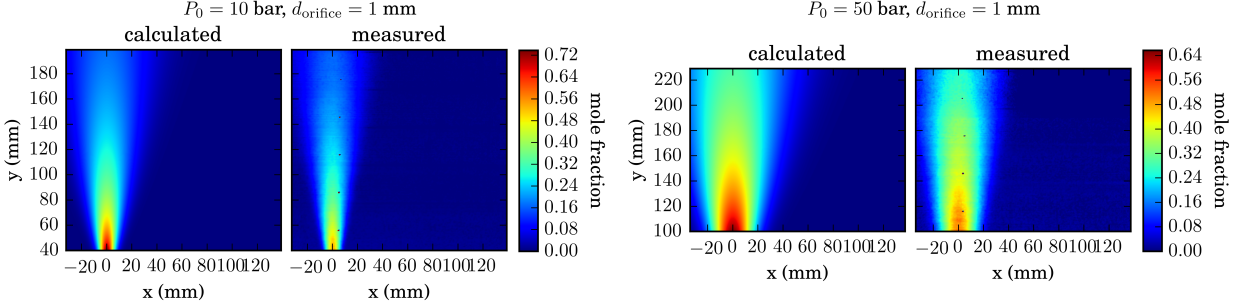


Figure 4: Predicted and PLRS measured mean mole fraction fields for a 1 mm orifice with a static pressure of 10 bar (left two images), and 50 bar (right two images).

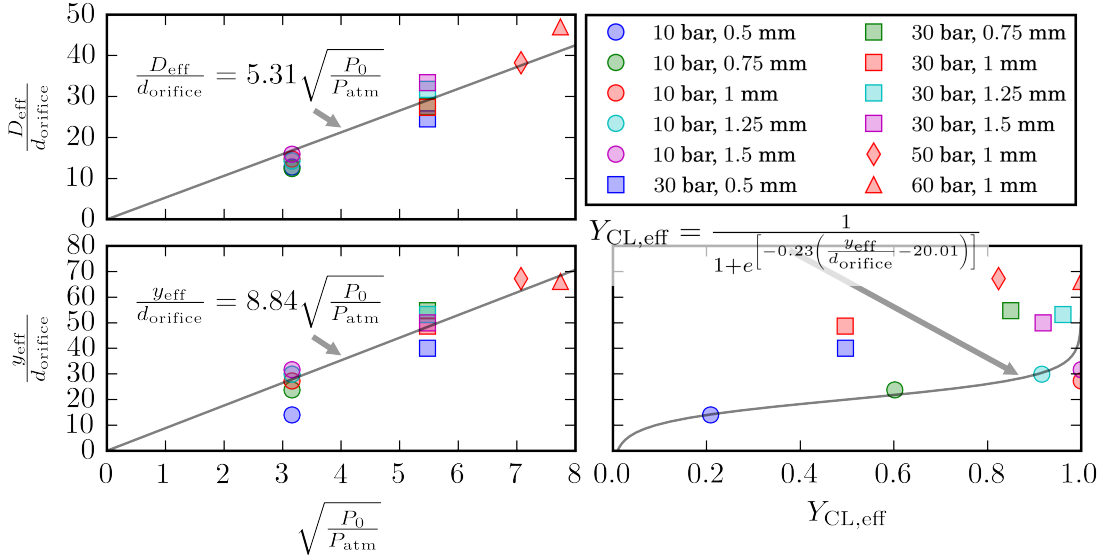


Figure 5: Effective leak diameter (upper left), starting point (lower left) and initial mole fraction hydrogen (lower right) for an under-expanded hydrogen jet. Fits to the data are also shown on the figure.

measurements of the velocity fields for these hydrogen jets, it is unclear whether this value, taken from historical work on water jets [25, 26], is appropriate. Yüceil and Ötügen [9] found that the spreading ratio of velocity to temperature for dried air was significantly higher (1.42) than the concentration spreading ratio used in this work. The entrainment sub-model may also not be appropriate for these hydrogen jets. Further measurements, especially of the velocity fields, could justify these (or assist in calculating more appropriate) model parameters.

Figure 5 shows the equivalent source model boundary conditions for minimizing the error in the mole fraction fields for all of the PLRS data. As with the Mach disk and slip region geometries for the under-expanded jet shown in Fig. 3, the effective diameter and starting point of the jet model scale linearly with respect to the square root of the pressure ratio. Rather than plotting the initial centerline density ( $\rho_{\text{cl},0}$ ) for the model, the initial mass fraction of hydrogen is plotted in the lower right frame of Fig. 5. For the smallest pressure ratios, the initial mass fraction approaches zero, meaning the jet is nearly pure air. As the pressure ratio increases, the starting centerline concentration becomes pure hydrogen (mass fraction of 1). There is significantly more scatter in

the initial centerline mole fraction than the starting position or the effective diameter. Nonetheless, up to the 60 bar static pressure for hydrogen, these correlations seem to hold true.

## 5 CONCLUSIONS

In this work, we presented schlieren images quantifying the geometry of the shock structure of under-expanded hydrogen jets up to 60 bar. As has been observed previously for the shock structure of under-expanded jets of other gases, the Mach disk location varies as the square root of the static to atmospheric pressure ratio. We offer linear fits to the Mach disk location, the Mach disk diameter, and the diameter of the slip region at the Mach disk downstream location as a function of the square root of the pressure ratio. These correlations can be used in notional nozzle models of the expansion-zone of under-expanded hydrogen jets.

We also present an equivalent source model that can be used to provide boundary conditions to a reduced-order jet model (or CFD model), after the complex shock structure of an under-expanded hydrogen jet. The boundary conditions needed for a first-order, subsonic, hydrogen jet model to match planar laser Rayleigh scattering data for the mole fraction of hydrogen jets, with up to 60 bar static pressure were calculated. Correlations are given for the initial centerline mole fraction of hydrogen, the initial plume model starting location, and the effective orifice diameter of a subsonic plume from that location. The boundary conditions to the model also scale (linearly for the effective diameter and standoff distances) with the square root of the pressure ratio. These correlations can be used confidently for predicting the concentration field of pressurized hydrogen leaks, up to 60 bar.

To use the correlations in this work confidently up to much higher pressures, such as the 700 bar tank pressures common on hydrogen fuel cell vehicles, testing at increased pressures is needed. More confidence in the correlations (and improved correlations) could be realized by also measuring the velocity field in the subsonic portion of these under-expanded hydrogen jets. Further work is also needed to understand the expansion region of high aspect ratio leaks, such as those that develop from extended cracks. While these leaks have also been shown to collapse onto the canonical decay curves for concentration and velocity fields, the same correlations given herein likely do not apply, without the proper scaling of the effective leak diameter.

Reduced order models can be a powerful tool to rapidly model hydrogen leak scenarios. This is especially useful when performing quantitative risk assessment where a large scenario space must be spanned. The equivalent source model in this paper provides an accurate, rapid method to generate boundary conditions to reduced order jet and flame models, enabling accurate and effective QRA.

## 6 ACKNOWLEDGMENTS

This research was supported by the United States Department of Energy Fuel Cell Technologies Office, under the Safety, Codes, and Standards subprogram element managed by Will James. Further support from the National Natural Science Foundation of China, Grant No. 51476091, is also appreciated. Finally, the authors are grateful for the financial support from China Scholarship Council. Sandia National Laboratories is a multi-program laboratory managed and operated by Sandia Corporation, a wholly owned subsidiary of Lockheed Martin Corporation, for the U.S. Department of Energys National Nuclear Security Administration under contract DE-AC04-94AL85000.

## References

- [1] Stations — California Fuel Cell Partnership. <http://cafcp.org/toolkits/stations>
- [2] A. P. Harris, D. E. Dedrick, C. Lafleur, C. S. Marchi, Safety , Codes and Standards for Hydrogen Installations : Hydrogen Fueling System Footprint Metric Development, Tech. Rep. SAND2014-3416, Sandia National Laboratories (2014).
- [3] J. LaChance, W. Houf, B. Middleton, L. Fluier, Analyses to support development of risk-informed separation distances for hydrogen codes and standards, Tech. Rep. SAND2009-0874, Sandia National Laboratories (2009).
- [4] C. H. Lewis, Jr., D. J. Carlson, Normal shock location in underexpanded gas and gas-particle jets, *AIAA J.* 2 (4) (1964) 776–777.
- [5] S. Crist, P. M. Sherman, D. R. Glass, Study of the highly underexpanded sonic jet., *AIAA J.* 4 (1) (1966) 68–71.
- [6] A. Birch, D. Brown, The structure and concentration decay of high pressure jets of natural gas, *Combust. Sci. Technol.* 36 (1984) 249–261.
- [7] B. C. R. Ewan, K. Moodie, Structure and Velocity Measurements in Underexpanded Jets, *Combust. Sci. Technol.* 45 (5-6) (1986) 275–288.
- [8] E. Rajakuperan, M. a. Ramaswamy, An experimental investigation of underexpanded jets from oval sonic nozzles, *Exp. Fluids* 24 (4) (1998) 291–299.
- [9] K. B. Yüceil, M. V. Ötügen, Scaling parameters for underexpanded supersonic jets, *Phys. Fluids* 14 (12) (2002) 4206–4215.
- [10] A. J. Ruggles, I. W. Ekoto, Ignitability and mixing of underexpanded hydrogen jets, *Int. J. Hydrogen Energy* 37 (22) (2012) 17549–17560.
- [11] A. J. Ruggles, I. W. Ekoto, Experimental investigation of nozzle aspect ratio effects on under-expanded hydrogen jet release characteristics, *Int. J. Hydrogen Energy* 39 (35) (2014) 20331–20338.
- [12] E. Papanikolaou, D. Baraldi, M. Kuznetsov, A. Venetsanos, Evaluation of notional nozzle approaches for CFD simulations of free-shear under-expanded hydrogen jets, *Int. J. Hydrogen Energy* 37 (23) (2012) 18563–18574.
- [13] A. Birch, D. Hughes, F. Swaffield, Velocity decay of high pressure jets, *Combust. Sci. Technol.* 52 (1987) 161–171.
- [14] K. Harstad, J. Bellan, Global analysis and parametric dependencies for potential unintended hydrogen-fuel releases, *Combust. Flame* 144 (1-2) (2006) 89–102.
- [15] V. Molkov, *Fundamentals of Hydrogen Safety Engineering I*, bookboon.com, 2012.
- [16] I. Ekoto, a.J. Ruggles, L. Creitz, J. Li, Updated jet flame radiation modeling with buoyancy corrections, *Int. J. Hydrogen Energy* 39 (35) (2014) 20570–20577.
- [17] T. C. Williams, C. R. Shaddix, Simultaneous correction of flat field and nonlinearity response of intensified charge-coupled devices, *Rev. Sci. Instrum.* 78 (12).
- [18] A. Velikorodny, S. Kudriakov, Numerical study of the near-field of highly underexpanded turbulent gas jets, *Int. J. Hydrogen Energy* 37 (22) (2012) 17390–17399.
- [19] K. Hatanaka, T. Saito, Influence of nozzle geometry on underexpanded axisymmetric free jet characteristics, *Shock Waves* 22 (2012) 427–434.
- [20] W. Houf, R. Schefer, Analytical and experimental investigation of small-scale unintended releases of hydrogen, *Int. J. Hydrogen Energy* 33 (4) (2008) 1435–1444.
- [21] I. H. Bell, J. Wronski, S. Quoilin, V. Lemort, Pure and pseudo-pure fluid thermophysical property evaluation and the open-source thermophysical property library coolprop, *Ind. Eng. Chem. Res.* 53 (2014) 2498–2508.
- [22] R. Storn, K. Price, Differential evolution a simple and efficient heuristic for global optimization

- over continuous spaces, *J. Glob. Optim.* (1997) 341–359.
- [23] D. J. Wales, J. P. K. Doye, Global Optimization by Basin-Hopping and the Lowest Energy Structures of Lennard-Jones Clusters Containing up to 110 Atoms, *J. Phys. Chem. A* 101 (28) (1997) 5111–5116.
- [24] X. Li, E. S. Hecht, D. Christopher, Validation of Reduced Models for Subsonic and Underexpanded Hydrogen Jets (In Preparation).
- [25] B. Gebhart, D. S. Hilder, M. Kelleher, The Diffusion of Turbulent Buoyant Jets, *Adv. Heat Transf.* 16 (1984) 1–57.
- [26] G. Abraham, Horizontal Jets in Stagnant Fluid of Other Density, *J. Hydraul. Div.* 91 (4) (1965) 139–154.